Article

Performance Evaluation of Harmonic Reduced Non-Overlap Winding Wound Rotor Synchronous Machine

Karen S. Garner *, Maarten J. Kamper and Andrew T. Loubser *

Department of Electrical and Electronic Engineering, Stellenbosch University, Stellenbosch 7600, South Africa; kamper@sun.ac.za
* Correspondence: garnerks@sun.ac.za (K.S.G.); atloubser@sun.ac.za (A.T.L.)

Abstract: The analysis and performance evaluation of a harmonic reduction strategy of a non-overlap winding wound rotor synchronous machine is conducted in this paper. The harmonic reduction strategy utilizes phase-shifts between coil currents to reduce sub- and higher-order harmonics. The design is performed on a 3 MW wound rotor synchronous machine with a 16/18 pole/slot combination. The application results in a lowered torque ripple and an increased efficiency of the designed machine. The manufacturing and testing of a 3 kW prototype to ascertain the effectiveness of the design is also presented. The practical measurements correlate successfully with the theoretical results.

Keywords: harmonic reduction; non-overlap; phase-shifting; star-delta; synchronous machine; wound rotor

1. Introduction

The drive to reduce costs and improve efficiency of electric machines in power generation applications, amongst others, is an ongoing study. Much focus has been applied to the renewable energy sphere to provide sustainable energy solutions to growing global power demands. Wind generation registered a growth of 10% from 2018 to 2019, according to the Renewables Global Status Report for 2019 [1]. Permanent magnet synchronous machines (PMSMs) have been the preferred solution for wind generation systems, partly because of the reduced size of the generator, but methods to improve other synchronous machines are in demand to avoid the use of rare-earth materials and reduce the cost of generation. This study focuses on a wound rotor synchronous machine (WRSM), attractive for, amongst other reasons, the ability to vary flux and thus its reactive power when directly connected to the electrical grid. A non-overlap winding structure is used for the WRSM to improve torque density of the machine and to lower manufacturing costs associated with winding complexity [2]. It is well-known, however, that non-overlap windings contain sub- and higher-order harmonics in the magneto-motive force (MMF) distribution [2]. Numerous strategies have been applied to non-overlap windings to eliminate or reduce sub-harmonic MMF content. The study in [3] theorizes that because of the difference in harmonic content between a single-layer and a double-layer winding, applying a multi-layer winding could potentially reduce sub-harmonics further. A four-layer winding was applied to the stator of a 10/12 pole/slot combination machine and an 8/9 pole/slot combination machine. Despite the obvious added cost and complexity of a four-layer winding, it was also concluded that the strategy reduced all the MMF harmonics, including the working harmonic. For example, the winding factor of the fourth harmonic of the 8/9 pole/slot machine decreased from 0.945 to 0.888 with the first version of the design and to 0.931 with the second version of the design.

The use of concentrated coils to improve the MMF waveform was first explored with distributed windings in [4]. The designed winding uses a combination of two turn numbers such that all slots have two coil sides with a ratio of N1/N2 turns. However, the improvement of the MMF waveform was not significant compared to the increased

winding complexity and manufacturing costs. Some studies show an improvement in the working harmonic of the prototypes in question [5–7]. Unfortunately, the method does not reduce higher-order harmonics and is limited to certain pole/slot combinations. Stator shifting is another technique that has been investigated to reduce sub- and higher-order harmonics and was applied to a 14/12 pole/slot machine where the number of stator slots is then doubled [8]. The winding is divided into two separate windings that are shifted mechanically by an angle and the coil pitch is modified from 1 slot to 2 slots. As such, the windings then overlap. This structure shows a decrease in the sub-harmonics, but the winding structure is no longer a non-overlap concentrated winding, and the benefits of the original winding are lost. The same concept of stator shifting is applied in [9], but without changing the structure to an overlap winding. The base winding is a single layer non-overlap winding of a 14/24 pole/slot combination machine. A second winding is applied with the same distribution of coils, but mechanically shifted from the base winding and the two windings are then connected in series. The study shows an elimination of the first harmonic and a vast reduction of the fifth harmonic in comparison to a 10/12 pole/slot combination, but higher-order harmonics are still present in the MMF spectrum. The pitch factor is also reduced which leads to a reduced winding factor. To overcome this reduction, the number of turns is increased which leads to increased copper losses. This has also only been implemented on the pole/slot combinations stated and no general rule is available for the method.

The intent of this research is to apply a harmonic reduction strategy to a non-overlap winding as in [10]. The method augments the concept of stator shifting. The work in [10] successfully applies the strategy to a 10/12 pole/slot machine, but does not provide a general approach for the harmonic reduction strategy for other pole/slot combinations. Previous research has shown that a mechanical displacement between the winding coils in a phase set alone is not sufficient to markedly decrease the sub-harmonics without reducing the distribution factor of the main harmonic. An electrical phase displacement between the winding coil currents of a phase set is necessary as well. Classical MMF harmonic analysis assumes that no phase shift exists between the currents of the coils in a phase set. Hence, applying a phase shift requires the development of a new winding factor or, more specifically, a new distribution factor as developed in [11].

This study applies the wye-delta coil-current phase-displacement technique to a large 3 MW 16/18 (or else 8/9) pole/slot combination WRSM presented for a medium-speed geared solution with a setup as proposed in [12]. This paper develops harmonic winding factors and considers the harmonic torques in a detailed analysis of the theoretical performance of the 3 MW machine. A finite element analysis model is built and simulated in the commercial tool ANSYS Maxwell. A 3 kW prototype with the proposed phase-shifted winding is manufactured and experimentally analysed for the first time to assist with the validation process.

2. Theoretical Harmonic Analysis

Classical harmonic analysis of a non-overlap winding assumes that all the coils in a phase set are in phase or, in other words, in series. Introducing an electrical phase-shift between the coils of a phase set requires a new approach to the analysis of the coil set.

2.1. Proposed 16/18 Phase-Shifted Non-Overlap Winding

A cross-section of the proposed 16/18 non-overlap winding is displayed in Figure 1. The 16/18 winding has two winding sections, W_s. The number of coils, u, per phase set is described by

$$u = \frac{Q}{mW_s},\tag{1}$$

where Q is the number of stator slots/coils, m is the number of phases and W_s is the number of winding sections. This yields $u = 3$ for the 16/18 non-overlap winding.
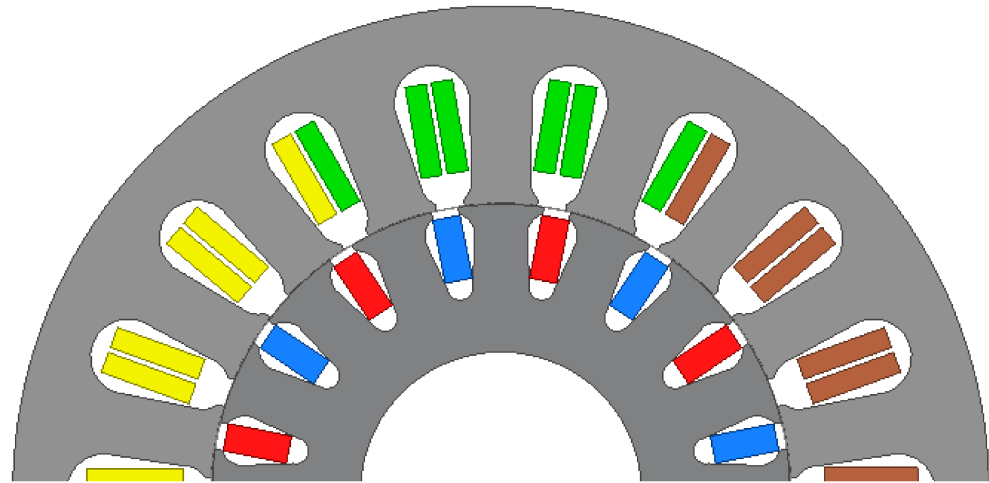
Figure 1. Cross-section of the 16/18 WRSM.

The conventional 16/18 non-overlap winding has all three coils of a phase group in series, as depicted in Figure 2a. The harmonic analysis of [11] explains that to achieve a distribution factor of unity for the working harmonic, $v = 4$, while also greatly diminishing the sub- and higher-order harmonics, the phase-shift required between the coils of the phase set is $-20°$. To negate the need for an additional current supply to achieve the phase-shift between the coils, the phase-shift is implemented by configuring the layout and connection of the coils. The closest phase-shift that can be achieved by manipulating the layout of the coils in the phase set is $-30°$, which results in a distribution factor of the working harmonic of 0.9899 while still decreasing the effect of the sub- and higher-order harmonics. The $-30°$ shift is created by instituting a physical wye-delta connection between the coils of each phase set, as seen in Figure 2b.
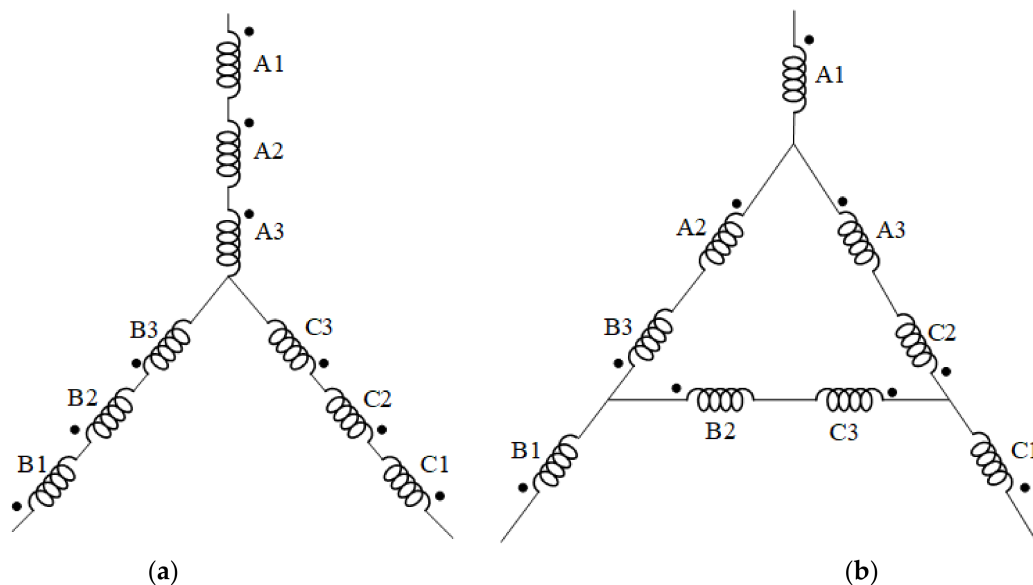

Figure 2. (**a**) Coil layout of a 16/18 conventional non-overlap winding; (**b**) Coil layout of the 16/18 phase-shifted non-overlap winding.

2.2. Harmonic MMF and Distribution Factor

In [11], a harmonic MMF function, F_{sv}, and a harmonic distribution factor, K_v, for the phase-shifted winding of Figure 2b above are described by

$$F_{sv} = \frac{3Nk_{pv}}{a\pi|v|} K_v I \sin(\omega t - v\theta - \beta) \tag{2}$$

and

$$K_v = \frac{\sqrt{(1 - \cos b - \cos c)^2 + (\sin c - \sin b)^2}}{u} \tag{3}$$

where

$$b = \alpha_2 - v\theta_s, \tag{4}$$

$$c = \alpha_3 - v\theta_s \tag{5}$$

and

$$\beta = \tan^{-1}\left(\frac{\sin c - \sin b}{1 - \cos b - \cos c}\right). \tag{6}$$

In Equations (1)–(4) the harmonic number is represented by v, N is the number of turns of each coil, k_{pv} is the pitch factor, a is the number of parallel paths in the winding, I is the peak amplitude of the phase current with rated q-axis current, and θ_s the electrical slot pitch angle given by

$$\theta_s = \frac{2\pi}{S}, \tag{7}$$

where S is the number of stator slots per machine section.

The angles α_2 and α_3 in Equations (4) and (5) are the required phase shifts of the second and third coil currents respectively and their total effect is represented by β. With $\alpha_2 = \alpha_3 = 0$ the coil currents are in phase as in the Y-connection of Figure 2a. With $\alpha_2 = \alpha_3 = -30°$ the coil currents are out of phase as in the Y-Δ connection of Figure 2b. It is shown in Table 1 that the distribution factors of the working and fifth harmonics are increased, but those of the other harmonics are notably reduced.

2.3. Flux Density and Torque Harmonic Analysis

It is necessary to investigate the effect of the phase-shift in terms of the harmonics of the air gap flux density as well as the torque harmonics. The air gap flux density harmonics are first determined due to the stator MMF and then in reference to the rotor MMF. The air gap flux density generated is determined from the stator MMF by

$$b_{sv} = \frac{\mu_0 F_{sv}}{g k_c} \tag{8}$$

Substituting Equation (2) into Equation (8),

$$b_{sv} = \frac{\mu_0}{g k_c} \frac{3Nk_{pv}}{a\pi|v|} K_v I \sin(\omega t - v\theta - \beta) \tag{9}$$

$$b_{rv} = \frac{\mu_0}{g k_c} \frac{3Nk_{pv}}{a\pi|v|} K_v I \sin(\omega_{rv} t - v\theta - \beta) \tag{10}$$

where the angle θ now refers to the rotor and the angular frequency ω_{rv} is given by

$$\omega_{rv} = \left(1 - \frac{2v}{p}\right)\omega. \tag{11}$$

It is noted from these equations that the changing winding factor will influence the air gap flux density harmonics. The only difference between Equations (9) and (10) is the angular frequency of the flux density and thus the amplitudes are the same. The effect of

the phase-shift can be seen in Figure 3 where the flux density of the working harmonic and the fifth harmonic is increased, while the sub- and higher-order harmonics are reduced. This is expected from the results of the winding factor presented in [11]. The percentage difference in the flux density between the conventional non-overlap and phase shifted winding is detailed in Table 1.
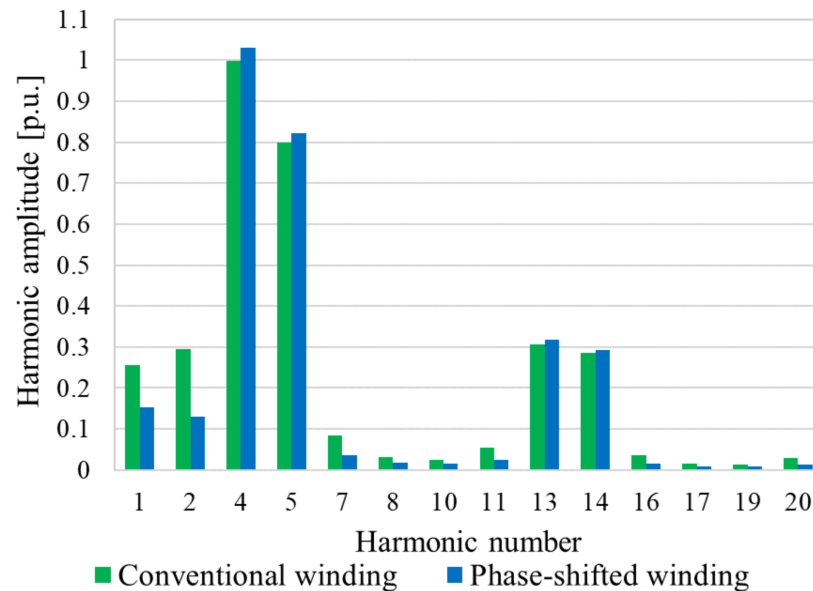

Figure 3. Per unit air gap flux density harmonics due to the stator MMF.

In a similar way as Equation (9) the air gap flux density harmonics created by the rotor field winding MMF are described by

$$b_{sv} = \frac{2\mu_0 p k_{prv}}{v \pi g k_c} K_{rv} I \cos\left(\frac{2v\omega t}{M_s p} - v\theta - \beta\right), \tag{12}$$

where k_{prv} and K_{rv} are the pitch factor and distribution factor of the rotor field winding respectively. These rotor winding factors are unchanged with the application of the phase shift in the stator winding and thus the flux density harmonics will remain the same. The rotor pitch factor is responsible for the presence of only harmonic multiples of the working harmonic.

Table 1. Air gap flux density harmonics of the 16/18 pole/slot conventional and phase-shifted non-overlap windings [11].

Harmonic Number	Air Gap Flux Density Harmonics in per Unit		
	Conventional 16/18 Winding	Phase-Shifted 16/18 Winding	% Difference
$v = 1$	0.2580	0.1532	−10.48
$v = -2$	0.2971	0.1300	−16.71
$v = 4$	1	1.0313	+3.13
$v = -5$	0.7968	0.8218	+2.49
$v = 7$	0.08262	0.0362	−4.65

The amplitude of the back-EMF induced voltage in the stator winding due to the rotor field can now be calculated as

$$E_{sv} = -\frac{16u\omega N l d_g B_{sv}}{vpM_s} K_v k_{psv}, \tag{13}$$

with

$$B_{sv} = \frac{2\mu_0 p k_{prv}}{v\pi g k_c} K_{rv} I. \tag{14}$$

Figure 4 shows the difference in the induced phase voltage between the two windings. Again, for the working harmonic the phase-shifted winding shows an increase (3.13%) over the conventional winding. This is expected because the induced phase voltage is directly proportional to the winding factor. The percentage of total harmonic distortion (THD) for the theoretical induced voltage is 2.15%.
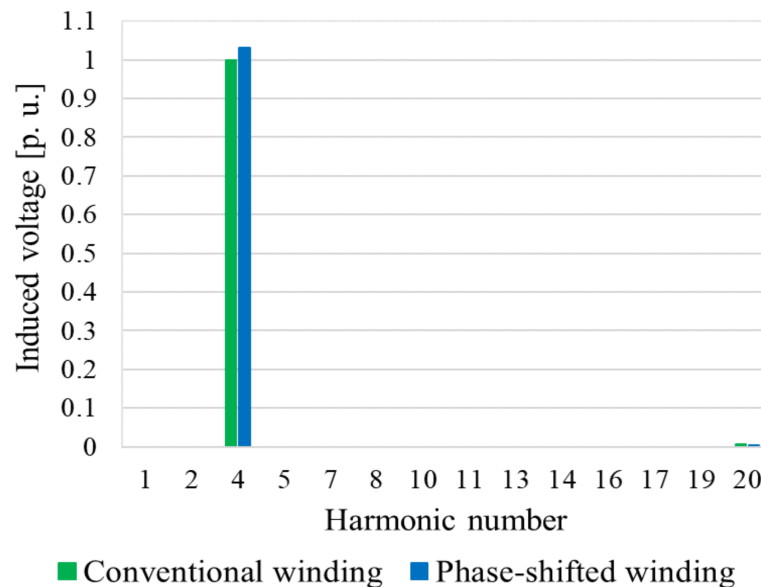

Figure 4. Induced phase voltage in the stator winding in per unit.

The instantaneous torque developed by the machine is described from the power developed by

$$T_s = \frac{pM_s}{2\omega} \sum_v [i_{abc}]^T \left[e_{abc(v)} \right], \tag{15}$$

where i_{abc} and $e_{abc(v)}$ are the phase currents and the induced voltages of the machine. With the phase current considered in phase with the induced voltage and thus only *q*-axis current available, this expression is further simplified as

$$T_s = \frac{3pM_s}{2\omega} I E_{s(p/2)} + \sum_j I \left(E_{s(j+1)p/2} + E_{s(j-1)p/2} \right) \cos(j\omega t), \\ j = 6, 12, 18, .. \tag{16}$$

The first term of Equation (16) is the average torque produced, while the second term refers to the oscillation or ripple of the developed torque. The theoretical torque profile of both winding structures is displayed in Figure 5. Only *j* = 6 is considered in the figure for illustrative purposes. The average torque of the phase-shifted winding shows an improvement of 3.13% as seen with the induced voltage. Figure 6 also shows that the torque ripple is suppressed by 11%, indicating the reduction of the sub- and higher-order harmonic content.
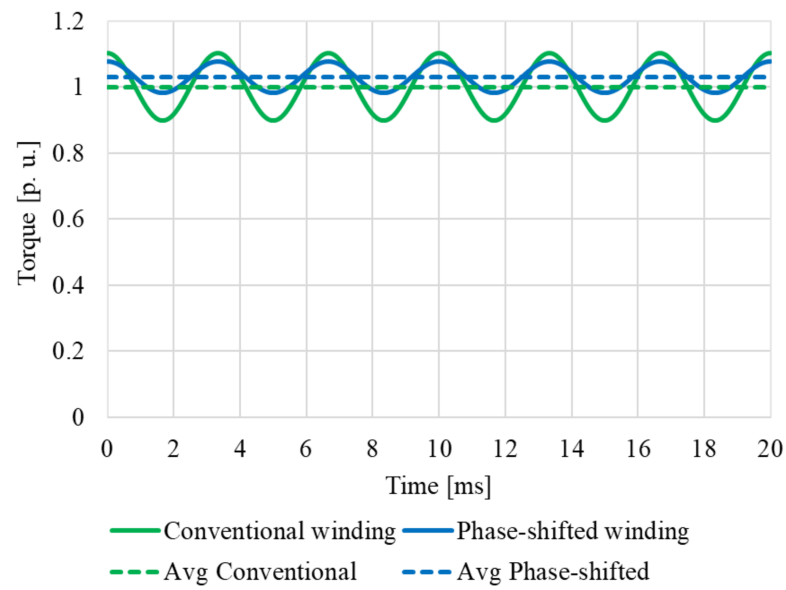
Figure 5. Comparison of the developed torque of the conventional and phase-shifted non-overlap windings.
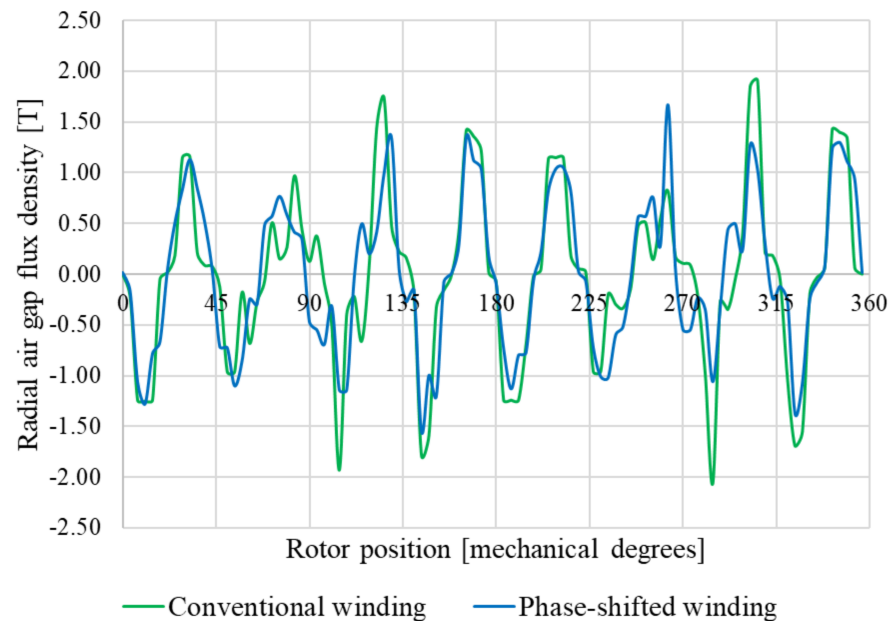

Figure 6. Simulated air gap flux density of the conventional and phase-shifted 16/18 non-overlap windings.

3. Simulated Performance Results

The specifications of the 3 MW generator used for the first investigation are stated in Table 2. The finite element analysis (FEA) simulated performance evaluation is conducted with rated q-axis current. The simulated air gap flux density of both winding structures is depicted in Figure 6. The air gap flux density of the phase-shifted winding is seen to be more consistent and prone to fewer fluctuations in amplitude because of the harmonic reduction. Further to this, Figure 7 displays the fourth harmonic component of both windings and confirms the dampening of the fluctuation.

Table 2. Specifications of the 3 MW 16/18 WRSM.

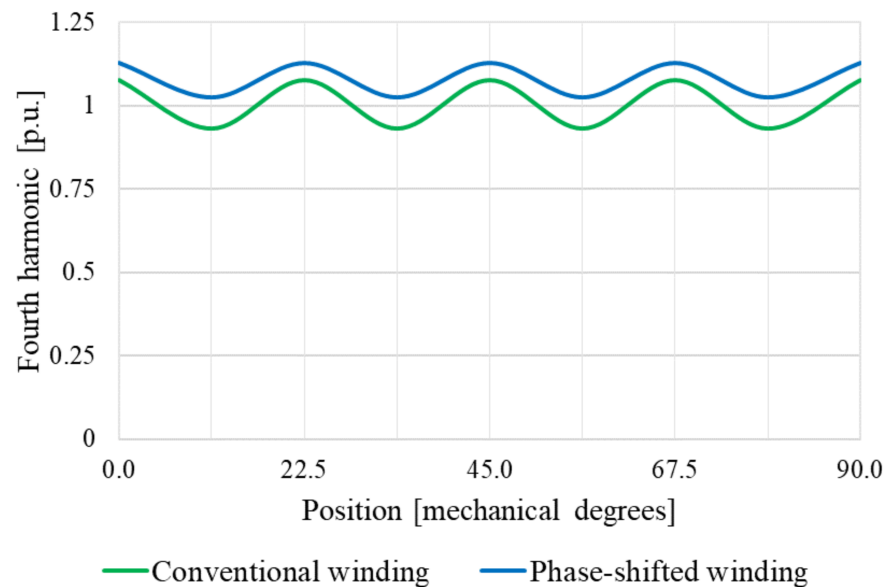| Specifications	Value
Rated terminal power (MW)	3
Rated torque (kNm)	76
Rated speed (r/min)	375
Rated frequency (Hz)	50
Rated line voltage (V)	580
Rated phase current (A)	3000
Rated field current (A)	200
Stator outer diameter (mm)	1600
Rotor outer diameter (mm)	981
Rotor inner diameter (mm)	460
Stack length (mm)	1500
Air gap length (mm)	3

Figure 7. Variation of the per unit fourth harmonic air gap flux density with rotor position of the conventional and phase-shifted 16/18 non-overlap winding machines.

Figure 8 shows the theoretical torque curves of the conventional and the phase-shifted 16/18 machines with a rated torque of 76 kNm. The average torque of the conventional winding is 75.36 kNm with a torque ripple of approximately 15.32%. The average torque of the phase-shifted winding is increased to 77.58 kNm and torque ripple is reduced to 9.53%. Further performance characteristics of the two machines are presented in Table 3. As is shown, the power output and efficiency of the machine are improved. The input current is the same for both cases, but the terminal voltage differs. The improved winding factor leads to an increased induced voltage. Although the total machines losses are reduced as a result of the overall reduction of sub-harmonics, the rotor core losses are increased after the implementation of the phase-shifting technique. This can be accredited to the improvement of, amongst others, the 5th harmonic's distribution factor.
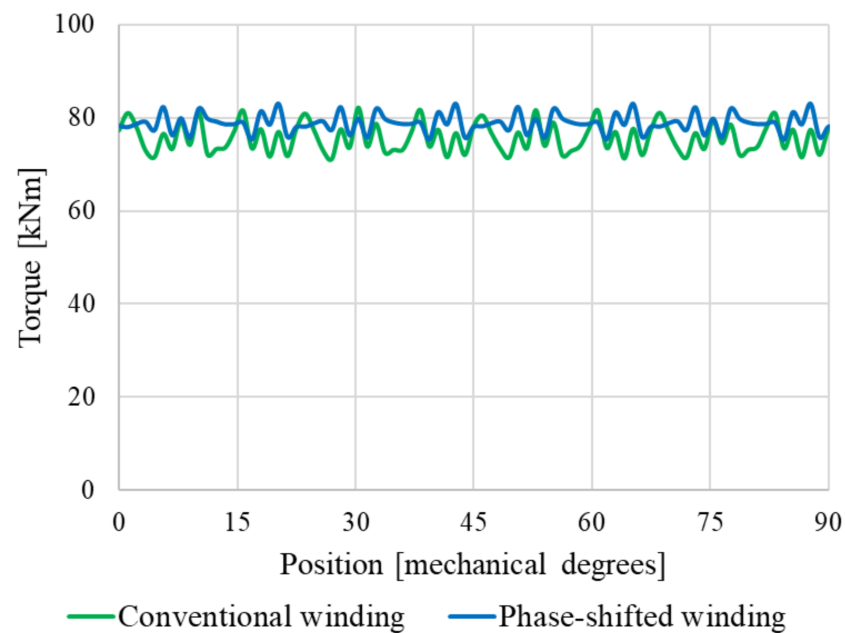
Figure 8. Torque curves of the conventional and phase-shifted 3 MW 16/18 winding machines.

Table 3. Performance of the conventional and phase-shifted winding machines.

Performance Parameter ↓	Conventional Winding	Phase-Shifted Winding	Percentage Difference
Terminal power (MW)	2.96	3.05	+3%
Shaft torque (kNm)	77.14	79.45	+3%
Torque ripple (%)	15.32	9.53	−5.79%
Rotor core loss (kW)	8.76	8.84	+0.91%
Stator core loss (kW)	25.58	23.19	−9.3%
Copper loss (kW)	43.08	43.08	−0%
Efficiency (%)	97.40	97.57	+0.17%

4. Measured Performance Results

A prototype of the design is required for the testing phase. Due to the impracticality of building a 3 MW prototype, the prototype of [13] was selected. The model was optimized using single line optimization to maximize the output torque. The model is not an exact scaled-down replica of the 3 MW prototype but serves to prove the concept of the harmonic reduction technique employed. The cross-section is displayed in Figure 9 and the specifications of the prototype are detailed in Table 4. The coil connections of the stator winding are completed on a terminal box. Figure 10 shows the test setup of the prototype for direct grid connection.

4.1. Machine Parameters from Tests

To confirm the characteristics of the prototype, the standard open-circuit and short-circuit tests are performed. Figure 11 displays the theoretical and experimental results of the open-circuit test of the 16/18 WRSM with phase-shifted non-overlap winding. The results of the short-circuit test are presented in Figure 12.

The equivalent circuit parameters of the 3 kW prototype are given in Table 5 and the measured machine losses are listed in Table 6. The windage and friction losses are determined with zero field current at the rated speed of 375 r/min. The core losses are determined by measuring the rotational losses at rated field current and rated speed and subtracting the measured windage and friction losses. The copper losses given are that of the stator winding at rated current.
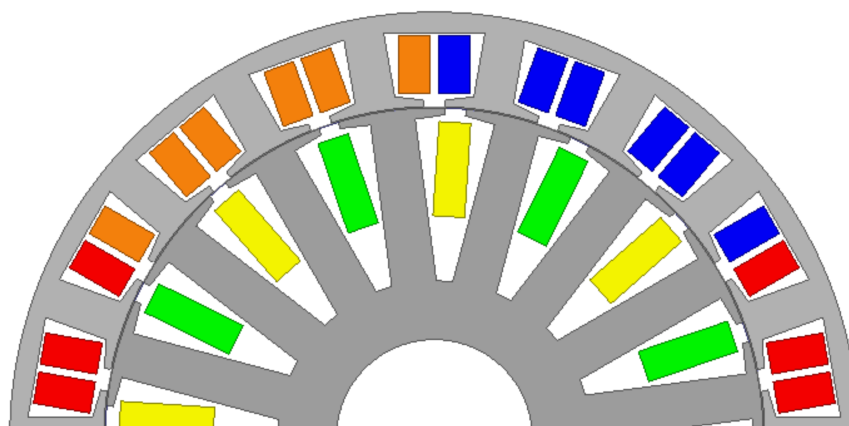
Figure 9. Cross-section of the 3 kW 16/18 pole/slot WRSM prototype.

Table 4. Specifications of the 3 kW 16/18 WRSM prototype.

| Specifications	Numerical Value
Rated terminal power (kW)	3
Rated torque (Nm)	76.5
Rated speed (r/min)	375
Rated frequency (Hz)	50
Rated line voltage (V)	350
Rated phase current (A)	4.86
Rated field current (A)	5.00
Number of rotor poles	16
Number of stator slots	18
Stator outer diameter (mm)	260
Rotor outer diameter (mm)	203.6
Rotor inner diameter (mm)	60
Stack length (mm)	125
Air gap thickness (mm)	0.45
Number turns per coil Y connected	67
Number turns per coil Δ connected	116
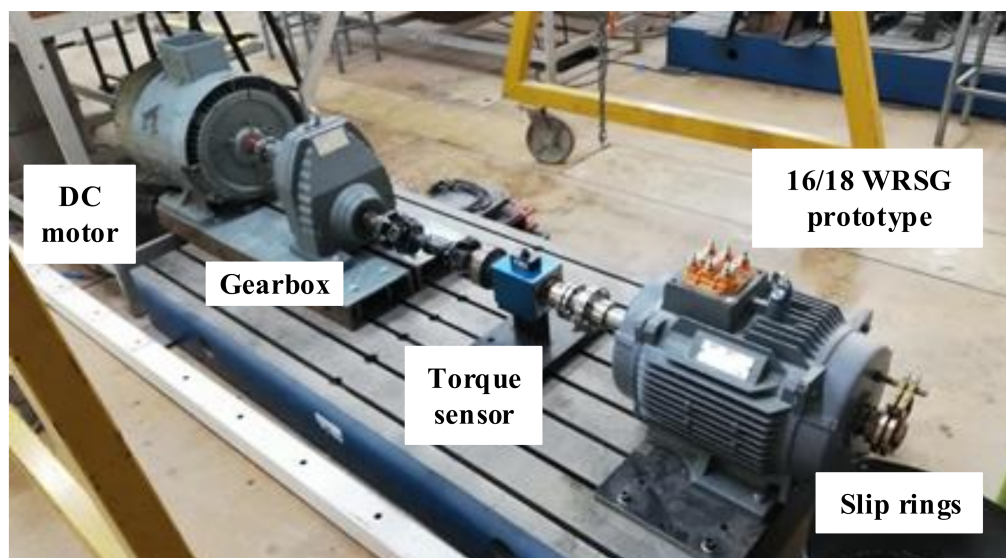
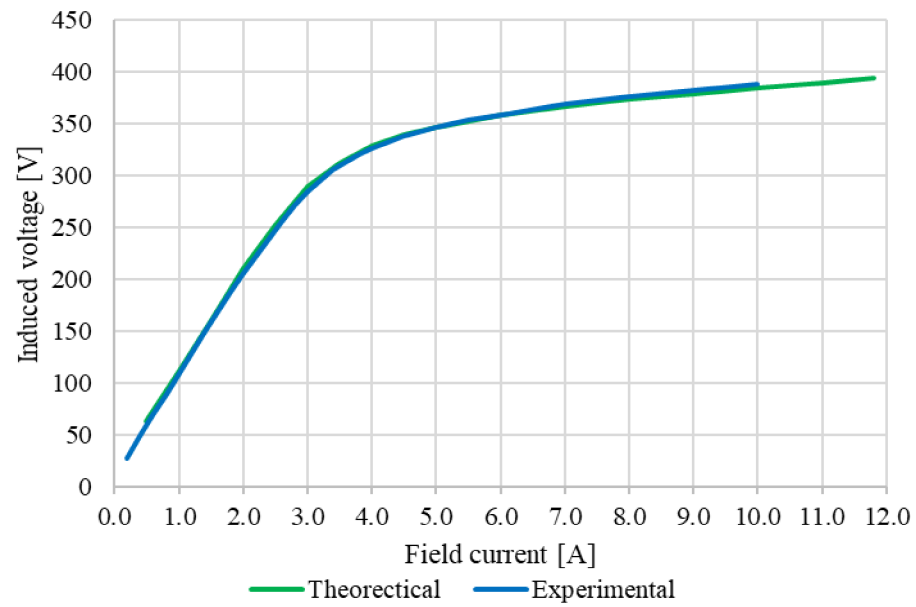**Figure 10.** Testing station of the 3 kW 16/18 pole/slot WRSM prototype.

Figure 11. Open-circuit line-to-line induced voltage versus field current of the non-overlap winding and phase-shift winding prototypes.
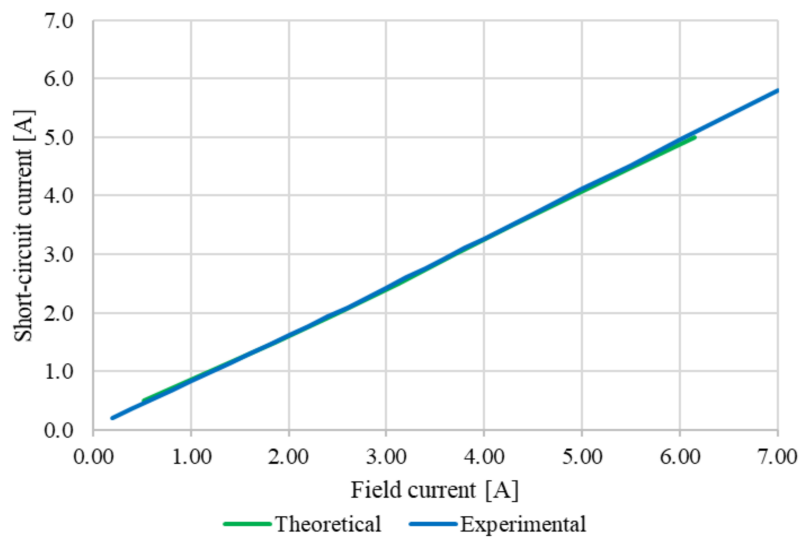

Figure 12. Predicted and experimental short-circuit current of the non-overlap winding and phase-shift winding prototypes.

Table 5. Measured equivalent circuit parameters of the phase-shifted winding prototype.

Parameter	Measured Value
Phase resistance, R_s	4.7 Ω (0.11 per unit)
Field resistance, R_f	8.1 Ω
Synchronous reactance, X_s	42.1 Ω (1.0 per unit)

Table 6. Measured machine losses of the phase-shifted winding prototype.

Windage and Friction Losses [W]	Core Losses [W]	Copper Losses [W]
19.6	62.8	94.5

4.2. Grid-Connected Tests

For the load performance tests the prototype is synchronised with the 50 Hz grid supply at the rated field current of 5 A. The mechanical input power is then increased by means of the DC motor in Figure 10, while also increasing the rotor field current to maintain unity power factor and grid synchronization. Figure 13 displays the measured power factor and field current versus generated electrical power. The phase-shifted winding machine is able to perform favourably and is able to maintain unity power factor until approximately 2.5 kW at a maximum field current of 10 A. Figure 14 displays the results of the efficiency and field current versus generated power of the machine. The results show the expected improved efficiency from the theoretical analysis. Figure 15 shows the predicted and experimental full-load torque curves of the prototype with the phase-shifted winding. The measured torque ripple is 8.2% and the results differ by 1.5%, which is an acceptable deviation. The measured full-load torque of the phase-shifted winding machine confirms the predicted improvements of the phase-shift application in terms of lowered torque ripple.

4.3. THD of Wye and Delta Phase Currents

It is necessary to determine to what extent circulating currents are present in the delta configuration of the phase-shifted non-overlap winding. With the machine open-circuited and at rated speed, the field current is varied and the current in a branch of the delta configuration is measured. The results are shown in Figure 16. As the field current increases, so too does the zero-sequence circulate current in the delta winding, though the circulating current remains relatively small (5.14% of the rated stator current at rated field current). A sample of the circulating current at rated field current at open circuit is displayed in Figure 17 and clearly illustrates the expected 150 Hz third harmonic characteristic.
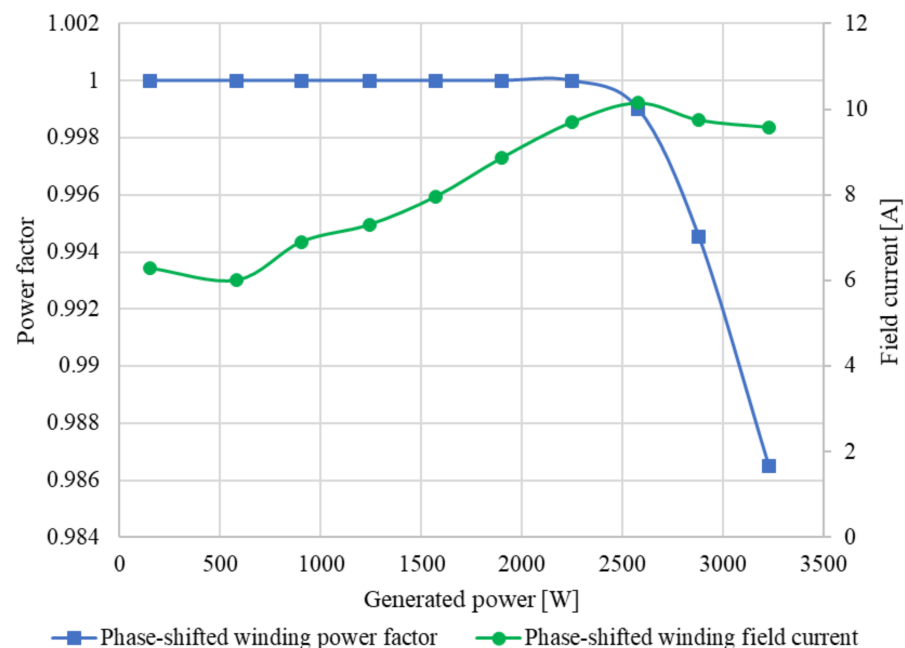

Figure 13. Power factor and field current versus generated power of the grid-connected phase-shift winding prototype.

The phase currents in the wye and the delta branches are shown in Figure 18 at a load phase current of 3.5 A and at unity power factor. The effect of the circulating current is clear on the delta phase current, which explains the presence of more harmonics when compared to the phase current in the wye branch. Further, the phase current waveforms in the different branches at a load phase current of 5 A and a power factor of $pF = 0.987$ are displayed in Figure 19. The total harmonic distortions (THD) of the wye and delta branch

currents for each of the three conditions are given in Table 7. This shows that the total harmonic distortion of the grid wye phase current is substantially below the 8% limit as required by some utility grid codes. In addition, the THD of the delta current reduces with load below the 8% and slightly higher than the THD of the grid wye current. For reference, the total harmonic distortion of the supply voltage during testing was 3%.
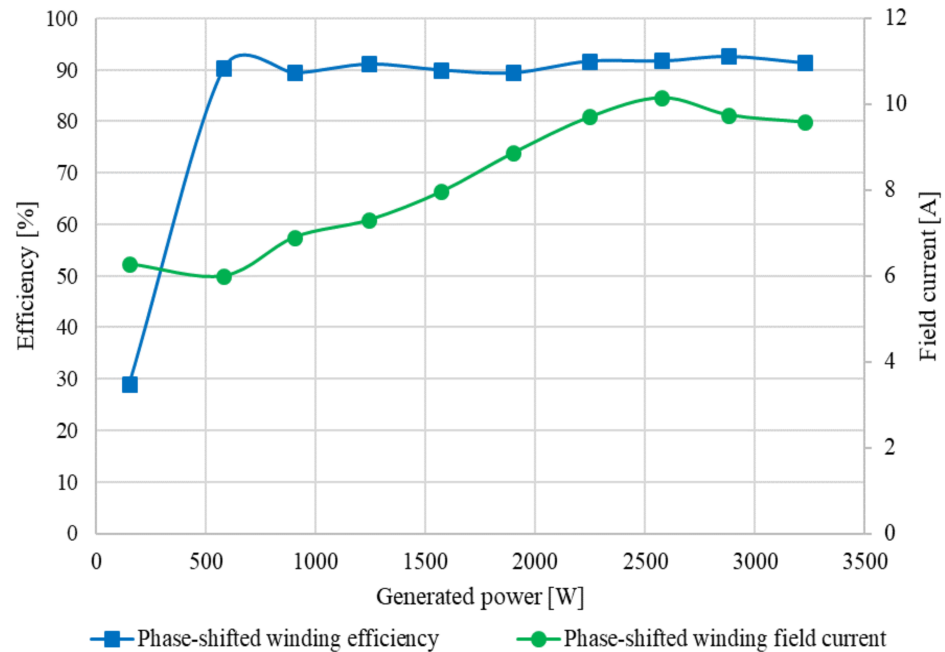

Figure 14. Efficiency and field current versus generated power of the grid-connected phase-shift winding prototype.
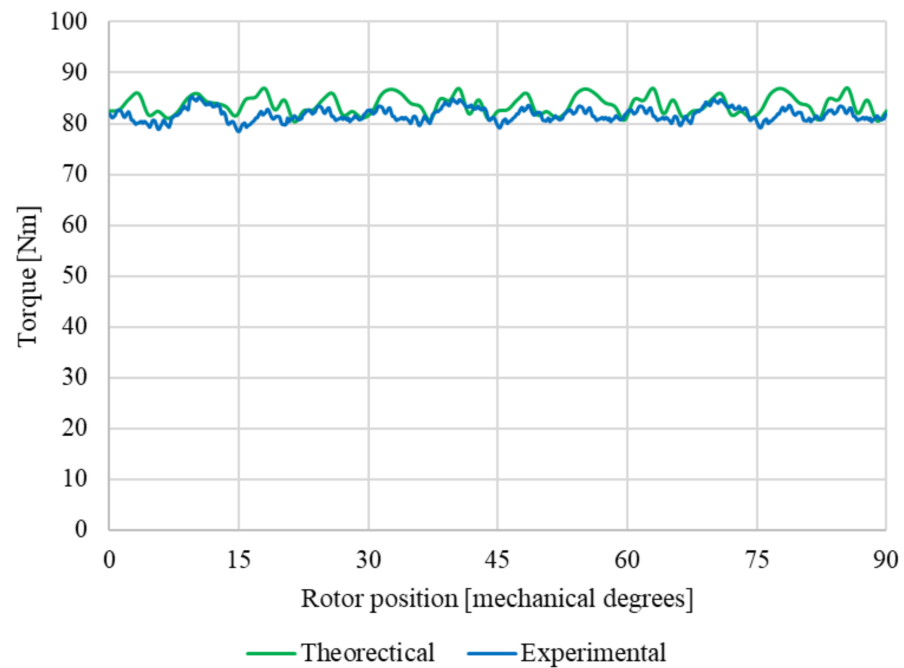

Figure 15. FEA-predicted and experimental torque versus rotor position of the 3 kW 16/18 WRSM prototype with phase-shifted non-overlap winding at 375 r/min and full-load.
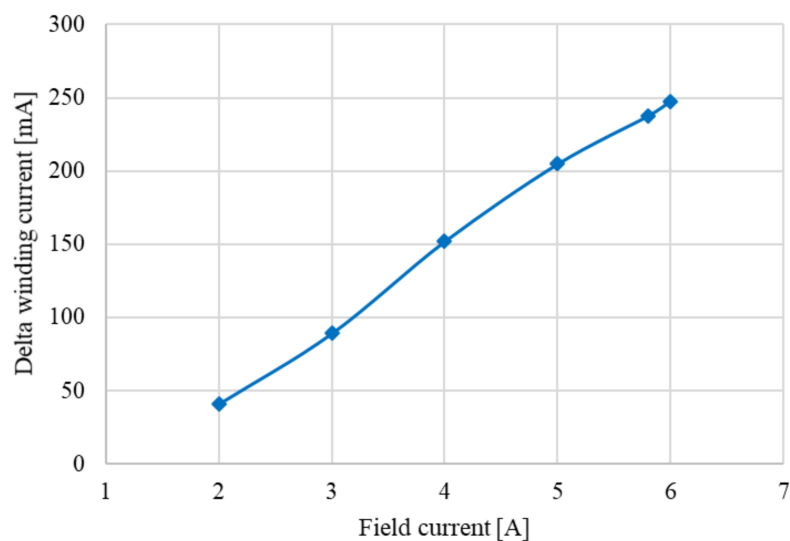
Figure 16. RMS delta winding current versus field current of the 3 kW 16/18 WRSG prototype with phase-shifted non-overlap winding at open-circuit.
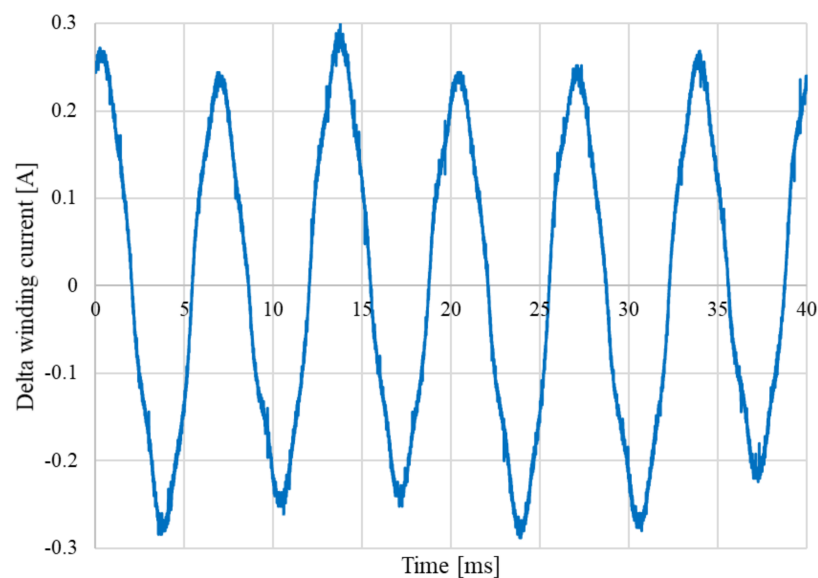

Figure 17. Delta winding circulating current at rated field current of the 3 kW 16/18 WRSG prototype with phase-shifted non-overlap winding at open-circuit.

Table 7. Total harmonic distortion of the wye and delta branch currents of the phase-shifted winding prototype with varying load conditions.

Load Condition			Wye Branch Current THD [%]	Delta Branch Current THD [%]
$I_s = 0$ A	$I_f = 5$ A	–	0	8.9
$I_s = 3.5$ A	$I_f = 10$ A	$pF = 1$	5.6	7.2
$I_s = 5$ A	$I_f = 9.6$ A	$pF = 0.987$	4.5	6.1

Figure 18. Grid-connected wye and delta phase currents at 3.5 A phase current and 10 A field current of the 3 kW 16/18 WRSG prototype with phase-shifted non-overlap winding at *pF* = 1.
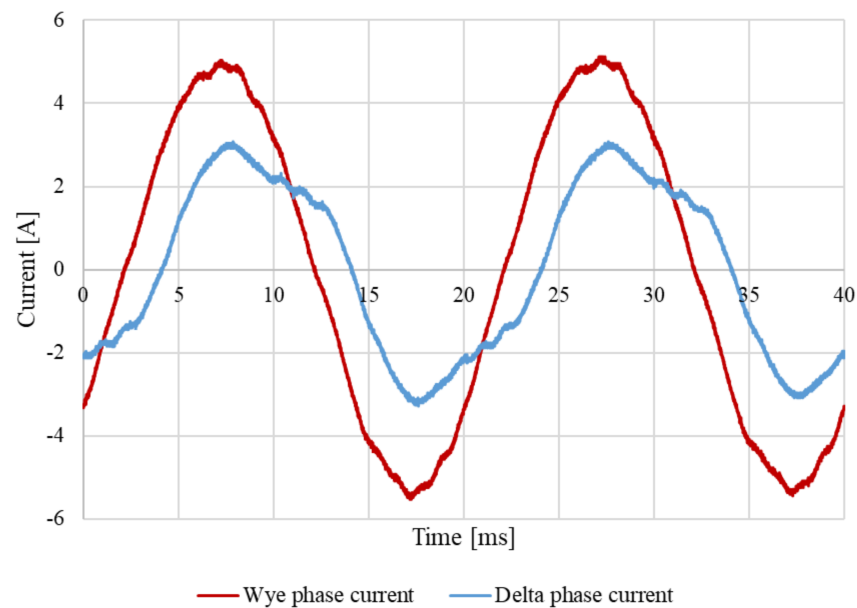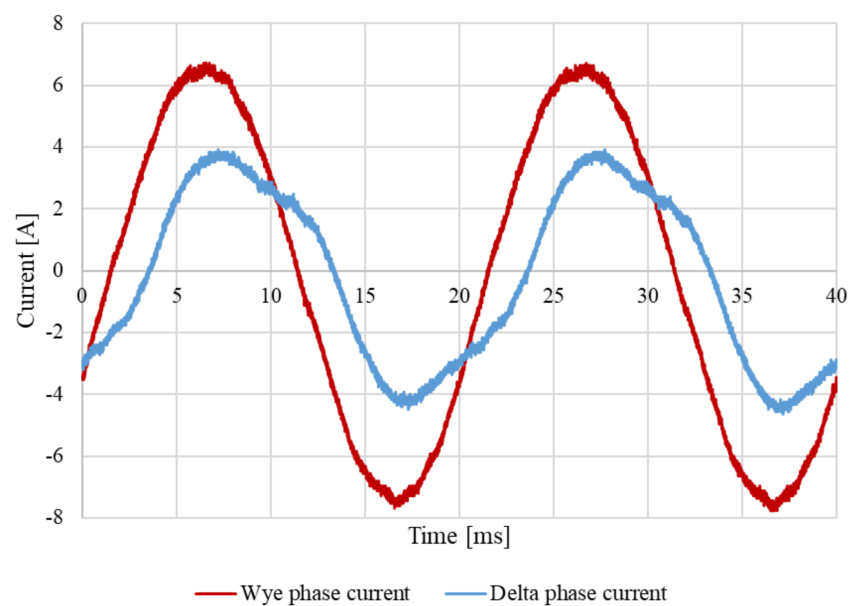

Figure 19. Grid-connected wye and delta phase currents at 5 A phase current and 9.6 A field current of the 3 kW 16/18 WRSG prototype with phase-shifted non-overlap winding at *pF* = 0.987.

5. Conclusions

In this paper the effect of the reduction of the MMF sub-harmonics of a 16/18 pole/slot combination WRSM on the performance of the machine by applying a phase-shifting winding technique, is studied. Ideally, a −20° electrical phase displacement is required between the currents of the coils to obtain a winding factor of unity of the main harmonic. To overcome the feasibility of applying this displacement practically, a −30° phase shift was selected which yields a winding factor close to unity. The phase shift was implemented by applying a star-delta connection between the coils of each phase. Although the wye-delta application is not new, the technique has not been applied to a 16/18 pole/slot combination before and the non-overlap winding structure is maintained. Many other techniques used to reduce the MMF harmonic content of a non-overlap winding change the final winding

structure to that of an overlap winding. This is not ideal because the advantages of the non-overlap winding are then diminished.

The harmonic content analysis of the 16/18 combination shows that the first and second MMF harmonics are greatly reduced without reducing the working harmonic. The winding factor of the main harmonic is increased by the phase-shift. This has improved the 16/18 machine's torque and power density. The minimization of sub- and higher-order harmonics is especially noted in the reduced torque ripple and increased efficiency of the phase-shifted winding machine. One of the disadvantages of the phase-shifted non-overlap winding is the small increase in the rotor core losses because of the increased 5th harmonic. However, the overall losses are reduced because the total sub-harmonic content is decreased.

A 3 kW prototype 16/18 WRSM with the proposed wye-delta phase-shifted non-overlap winding is manufactured and tested. The practical performance tests of this small machine indicate that the phase-shifted winding prototype has a good efficiency of over 90% for a wide power range from 0.2–1.0 per unit power. Additionally, the good full-load torque quality of the machine is confirmed by measurements. This all is expected from the reduction of sub- and higher-order harmonics in the MMF harmonic spectrum. Finally, the concern of possible high circulating current in the delta winding is studied from the measured delta current waveforms. The relatively low percentage THD found of the delta current from no-load to full load shows that this aspect is not a problem. In its entirety, the paper shows that the proposed non-overlap wye-delta phase-shift winding can be used with significant improvement by the industry for multiples of 8/9 pole-slot combination WRSMs.

Author Contributions: Conceptualization, K.S.G. and M.J.K.; methodology, K.S.G.; software, K.S.G.; validation, K.S.G. and M.J.K.; formal analysis, K.S.G.; investigation, K.S.G.; resources, K.S.G. and M.J.K.; data curation, A.T.L.; writing—original draft preparation and editing, K.S.G.; writing—review, M.J.K.; visualization, K.S.G. and M.J.K.; supervision, M.J.K.; project administration, K.S.G., M.J.K. and A.T.L.; funding acquisition, K.S.G. All authors have read and agreed to the published version of the manuscript.

Institutional Review Board Statement: Not applicable.

Informed Consent Statement: Not applicable.

Data Availability Statement: The data presented in this study are available within this study.

Conflicts of Interest: The authors declare no conflict of interest. The funders had no role in the design of the study; in the collection, analyses, or interpretation of data; in the writing of the manuscript, or in the decision to publish the results.

References

1. REN 21. Renewables 2019 Global Status Report (Paris: REN21 Secretariat). 2019. Available online: www.ren21.net/gsr (accessed on 10 October 2021).
2. Dajaku, G.; Spas, S.; Dajaku, X.; Gerling, D. An Improved Fractional Slot Concentrated Winding for Low-Poles Induction Machines. In Proceedings of the 19th International Conference for Electrical Machines, Lausanne, Switzerland, 4–7 September 2016; pp. 116–121.
3. Alberti, L.; Bianchi, N. Design and tests on a fractional-slot/induction machine. In Proceedings of the IEEE Energy Conversion Congress and Exposition (ECCE), Raleigh, NC, USA, 15–20 September 2012; pp. 166–172.
4. Heller, F.; Kauders, W. The Görges Polygon (Das Görgessche Durchflutungspolygon). *Arch. Elektrotechnik* **1925**, *29*, 599–616. [CrossRef]
5. Cistelecan, M.V.; Ferreira, F.J.T.E.; Popescu, M. Three phase tooth-concentrated multiple-layer fractional windings with low space harmonic content. In Proceedings of the 2010 IEEE Energy Conversion Congress and Exposition (ECCE), Atlanta, GA, USA, 12–16 September 2010; pp. 1399–1405.

6. Dotz, B.; Gerling, D. Windings with various numbers of turns per phasor. In Proceedings of the 2017 IEEE International Electric Machines and Drives Conference (IEMDC), Miami, FL, USA, 21–24 May 2017; pp. 1–7.

7. Dajaku, G.; Xie, W.; Gerling, D. Reduction of low space harmonics for the fractional slot concentrated windings using a novel stator design. *IEEE Trans. Magn.* **2014**, *50*, 1–12. [CrossRef]

8. Dajaku, G.; Gerling, D. A novel 24-slots/10-poles winding topology for electric machines. In Proceedings of the 2011 IEEE International Electric Machines Drives Conference (IEMDC), Niagara Falls, ON, Canada, 15–18 May 2011; pp. 65–70.

9. Zhu, S.; Shaohong, S.; Cox, T.; Xuand, Z.; Gerada, C. Novel 24-slots 14-poles fractional-slot concentrated winding topology with low-space harmonics for electrical machine. *J. Eng.* **2019**, *17*, 3784–3788. [CrossRef]

10. Bekka, N.; Trichet, D.; Bernard, N.; Zaïm, M. Application of Phase Shifting Technique for Reducing the Magnetomotive Force Space Harmonics of Tooth Concentrated Windings. *Electr. Power Compon. Syst.* **2016**, *44*, 1707–1720. [CrossRef]

11. Garner, K.S.; Kamper, M.J. Reducing MMF harmonics and core loss effect of non-overlap winding wound rotor synchronous machine (WRSM). In Proceedings of the IEEE Energy Conversion Congress and Exposition (ECCE), Cincinnati, OH, USA, 1–5 October 2017; pp. 1850–1856.

12. Ockhuis, D.K.; Kamper, M.J. Grid Connection Power Converter and Speed Controller for Slip-Synchronous Wind Generators. In Proceedings of the 2019 IEEE Energy Conversion Congress and Exposition (ECCE), Baltimore, MD, USA, 29 September–3 October 2019; pp. 6741–6748.

13. Kloppers, C.; Garner, K.S.; Kamper, M.J. Design and optimisation of a 16/18 wound rotor wind synchronous generator with non-overlap winding. In Proceedings of the 26th Southern African Universities Power and Engineering Conference, Johannesburg, South Africa, 24–26 January 2018; pp. 1–6.